Deformation Mechanisms of γ' and γ'' Co-precipitates in IN718

Longsheng Feng, Donald McAllister, Christopher H. Zenk, Michael J. Mills, and Yunzhi Wang

Abstract

Alloy 718 is widely used in gas turbine engines. Even though recent studies have been focusing on the unique deformation mechanisms of the tetragonal γ'' phase as compared to those of the cubic γ' phase, γ' and γ'' often co-precipitate and form composite particles. The deformation mechanisms of these composite particles have not been investigated in detail. In this work, we use a combination of ab initio and microscopic phase field methods to study shearing of a dual-lobed type $\gamma''/\gamma'/\gamma''$ composite particle by various dislocations. Complicated fault structures within both γ' and γ'' phases are predicted, and some of them have been observed in the experiment. The difficulty associated with experimental characterization of the fault structures in the co-precipitates is also discussed.

Keywords

IN718 • Precipitate shearing • Generalized stacking fault energy

Introduction

Alloy 718 is one of the most widely used materials in gas turbine industry [1–3]. While being formable and weldable with little hardening, the alloy exhibits superior mechanical properties at elevated temperatures up to 650 °C with appropriate aging treatment (like aeronautical aging, 8 h/720 °C + 8 h/620 °C). There are two primary strengthening phases, γ' ($L1_2$, cubic) and γ'' ($D0_{22}$, tetragonal). The γ'' phase forms lenticular particles with their minor axes parallel to $\langle 001\rangle_{\gamma''}$ [1]. Both γ' and γ'' phases have a cube-on-cube orientation relationship with the γ (FCC) matrix, and all three phases share the same slip system {111} <110>. This allows dislocations to shear continuously through the multi-phase microstructure in the alloy. The deformation mechanisms of each individual phase have been investigated both experimentally [4–6] and computationally [7–10]. Anti-phase domain boundaries (APB) and stacking fault ribbons have been observed in the deformed γ' microstructures. Phase field simulations have revealed the unique deformation pathways leading to these deformation microstructures. For the deformation of the γ'' phase, early studies have proposed APB shearing by a pair of like-signed $a/2$ <110> dislocations for one of the three variants and by a group of four like-signed $a/2$ <110> dislocations for the other two variants [11]. Formation of intrinsic stacking fault (ISF) within both the γ'' precipitates and γ matrix and microtwinning in overaged γ'' particles have been reported [12]. However, a recent study has showed that the shearing processes of γ'' precipitates could be much more complicated than those reported in the literature as well as those of the γ' phase because of the unstable stacking faults associated with the low symmetry $D0_{22}$ structure [10].

Depending on alloy composition and heat treatment schedule, the γ' and γ'' phases can form either monolithic or composite particles (i.e., γ' + γ'' co-precipitates) [13, 14]. Recent experiments have shown various types of co-precipitates including single-lobed, double-lobed (so-called sandwich structure), or compact configurations [6, 15, 16]. Comparing to the monolithic counterparts, some of these composite particles seem to have improved thermal stability in the prolonged aging [14, 17], which may lead to even better mechanical properties. This also raises a critical question on how these co-precipitates deform. The interplay between the deformation processes of the γ' and γ'' phases in a co-precipitate could certainly impact the overall

L. Feng · D. McAllister · C. H. Zenk · M. J. Mills · Y. Wang (✉)
Department of Materials Science and Engineering, The Ohio State University, 2041 College Rd, Columbus, OH 43210, USA
e-mail: wang.363@osu.edu

S. Tin et al. (eds.), *Superalloys 2020*, The Minerals, Metals & Materials Series,
https://doi.org/10.1007/978-3-030-51834-9_65

deformation behavior of the alloy. In this study, we perform microscopic phase field simulations, with ab initio calculations of the generalized stacking fault (GSF) energy as input, to study this interplay in a dual-lobed co-precipitate (Fig. 1). Dislocations of four different configurations are considered, which are a single *a*/2 <110> dislocation, a pair of like-signed *a*/2 <110> (CA + CA in the Thompson notation, total Burgers vector *a* <110>) dislocation group, a pair of unlike-signed *a*/2 <110> (total Burgers vector *a*/2 <112>) dislocation group, and two sets of *a*/2 <112> dislocation group (total Burgers vector *a* <112>).

Method

Microscopic Phase Field Model

Microscopic phase field model [18] is adopted to describe the interaction between dislocations and precipitates. In the model, dislocation loops are treated as the boundaries between sheared and unsheared regions on a glide plane and the sheared regions are characterized by a set of non-conserved order parameters, $\eta_p(\mathbf{r})$, where p represents the slip systems and $\mathbf{r}$ is the spatial coordinate [18]. In FCC crystals, any displacement caused by dislocation glide on <111> slip plane can be expressed as [9, 10]:

$$\mathbf{b} = \eta_1\mathbf{b}_1 + \eta_2\mathbf{b}_2 + \eta_3\mathbf{b}_3 \tag{1}$$

where $\mathbf{b}_1 = [10\bar{1}]/2$, $\mathbf{b}_2 = [\bar{1}10]/2$, and $\mathbf{b}_3 = [0\bar{1}1]/2$, and η_1, η_2, and η_3 are the magnitude of the inelastic displacement along the corresponding Burgers vectors. Time evolution of the order parameters $\eta_p(\mathbf{r})$ follows the time-dependent Ginzburg–Landau (TDGL) equations:

$$\frac{\partial \eta_p}{\partial \tau} = -L_p \frac{\delta F}{\delta \eta_p} \quad p = 1, 2, 3 \tag{2}$$

where τ is the dimensionless time, L_p is the kinetic coefficient characterizing dislocation mobility, and F is the total free energy of the system, which is composed of three parts [9, 10]: crystalline energy E^{crystal}, gradient energy E^{grad} and elastic energy E^{elast}, i.e.,

$$F = E^{\mathrm{crystal}} + E^{\mathrm{grad}} + E^{\mathrm{elast}} \tag{3}$$

The crystalline energy is sometimes referred as the generalized stacking fault energy (GSFE), which usually comes from atomistic simulations.

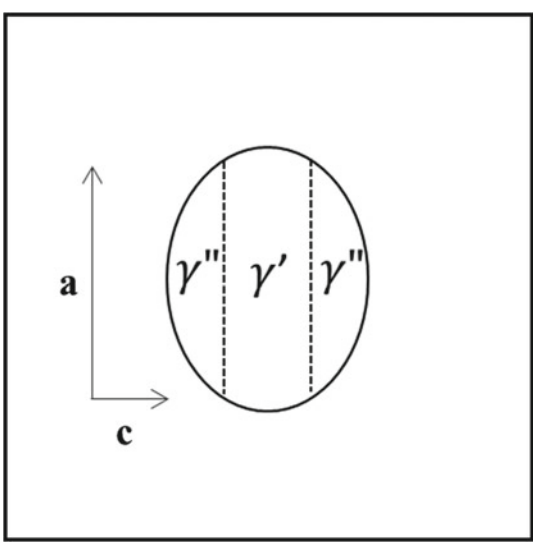

Fig. 1 Dual-lobed precipitate used in the phase field simulation. The **c axis** and **a** axis are also labeled

GSF Energy Landscape of γ' and γ'' Phases

For the sake of simplicity, the GSF potential energy surface of the γ matrix (FCC) is approximated by that of pure Ni. Since precipitation hardening by the γ' and γ'' phases are much stronger than the Peierls stress, this simplification will not change the conclusions of this study on the dominant deformation mechanisms. The GSF energy surface of γ, γ'' phases is taken from [10], and GSF energy of γ' phase is taken from [8]. Figure 2 shows the GSF energy landscape of γ' and γ'' phases. It should be noted that even though both phases have complex-stacking-faults (CSF), superlattice-intrinsic-stacking-fault (SISF), and APB fault, their fault energies are distinctively different. From the GSF energy landscape, fault structures that can be created by a single *a*/6 <112> dislocation are either CSF or ISF. The ISF is a stable configuration with an extremely low energy ($\sim$2.3 mJ/m^2) [10], while the CSF is an unstable configuration with a significantly higher energy. Similarly, two fault structures, APB (stable) and APB-like (unstable), could be created by *a*/2 <110> dislocations. It has been shown that the stable APB is difficult to form in the γ'' phases due to its high energy whereas the unstable APB-like will transforms itself into ISF by nucleating a remnant Shockley partial [10]. This is drastically different from the case in the γ' phase where any *a*/2 <110> dislocations would lead to a stable APB structure. Since both the CSF and APB-like configurations are unstable in the γ'' phase, once created, they will transform spontaneously into nearby stable faults on the GSF energy surface. So, the simple APB shearing mechanism proposed in the literature [11] does not operate in 2/3 of the γ'' precipitates. As will be shown later, the unstable nature of the CSF and APB-like faults plays a critical role in dominating the deformation processes of γ'/γ'' co-precipitates.

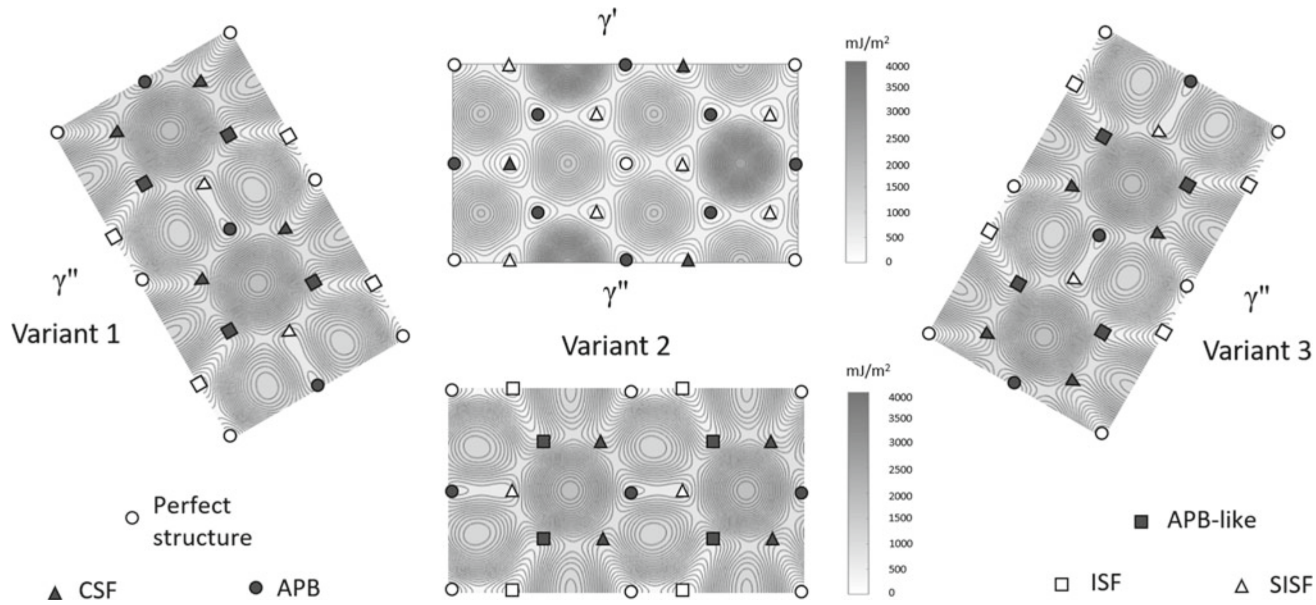

Fig. 2 GSF energy landscape of {111} plane of γ' and γ'' phases

Results

Shearing of a Dual-Lobed Co-precipitate by *a*/2 <110> Dislocations

There are six $a/2$ <110> dislocations on {111} plane in both γ' and γ'' phases. Considering the symmetry of the crystal, all six dislocations are equivalent in the γ' phase, whereas three of them are distinctively different in the γ'' phase. AC, AB, and CA dislocations (in Thompson notation) are studied, respectively, on their interactions with the dual-lobed co-precipitate. All simulations are performed under an applied stress of 800 MPa along the total Burgers vector direction.

Figure 3a shows the interaction between an AB dislocation and the dual-lobed co-precipitate. Due to the high APB energy in the γ'' phase, the whole particle is looped by the dislocation, even though APB in the γ' phase particle will occur if it is not in such a co-precipitate configuration. Figure 3b shows the interaction between an AC dislocation and the dual-lobed co-precipitate. In the γ' phase, the AC dislocation creates an APB. In the γ'' phase, due to the high-energy APB-like fault, only the leading partial δC of AC shears the γ'' phase, creating an ISF. The trailing partial Aδ of AC loops the γ'' particle. Unlike the previous case, the γ'' phase does not stop the full AC dislocation enter the co-precipitate. On the contrary, due to the extremely low energy of the ISF created by leading partial Aδ, Aδ will drag the whole AC dislocation through the γ' phase. The high CSF energy in the γ' phase also prevents the decorrelation of Aδ and δC in the γ' phase, which leads to the formation of APB in this case. The final deformation microstructure is APB in γ' and ISF in γ'', with a Shockley partial looping around the γ'' particle (Frame 3). The deformation pathway is plotted with solid light gray arrows on the GSF energy counter shown in Fig. 4. Figure 3c shows the interaction between a CA dislocation and the dual-lobed particle. The CA dislocation creates an APB in the γ' phase and an APB-like fault in the γ'' phase (Frame 2). A remnant Shockley partial δB is nucleated in the γ'' phase instantaneously, transforming the APB-like unstable fault into an ISF (Frame 3). Then, the partial δB propagates into the γ' phase, transforming APB into SISF (Frame 4). The final deformation microstructure is an SISF in the γ' phase and an ISF in the γ'' phase, with a Shockley partial δB looping around the whole co-precipitate. The deformation pathways in both γ' and γ'' phases are plotted by the dark gray arrows on the GSF energy counter plot shown in Fig. 4. The remnant Shockley partial δB is represented by the dash dark gray arrow.

Shearing of a Dual-Lobed Co-precipitate by an *a* <110> Dislocation Group (i.e., CA + CA)

Figure 5 shows the interaction between the dual-lobed co-precipitate with a second CA dislocation, assuming the first CA dislocation has already passed. Due to the existence of a remnant Shockley partial δB, the trailing partial Cδ of the second CA cuts the γ' phase first, transforming the SISF into an APB (Frame 2). Then, the leading partial δA and the remnant partial δB cut into the γ' phase and restore a perfect crystal structure (i.e., without any fault) in the γ' phase. In the γ'' phase, the trailing partial Cδ of CA restores a perfect crystal structure in the γ'' phase, while the leading partial δA

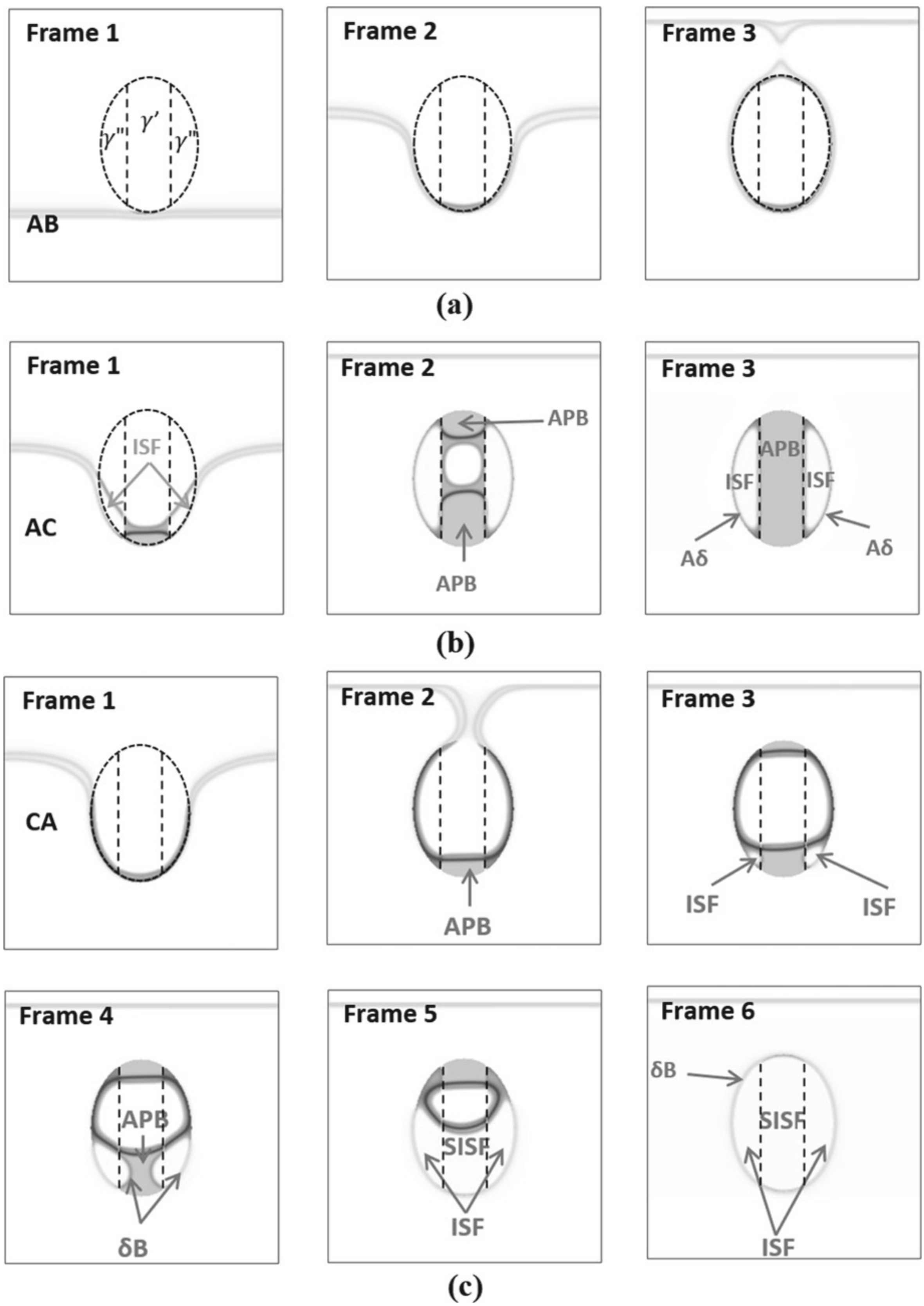

Fig. 3 Interaction between **a** AB, **b** AC, and **c** CA dislocations with a dual-lobed co-precipitate (shown in Fig. 1). The three frames in each row are snapshots capturing the whole deformation process. The crystalline energy contour is plotted, the darker the color, the higher the energy. The black ellipse indicates the interface between the co-precipitate and matrix, while the black dash line indicates the interface between γ' and γ'' phases

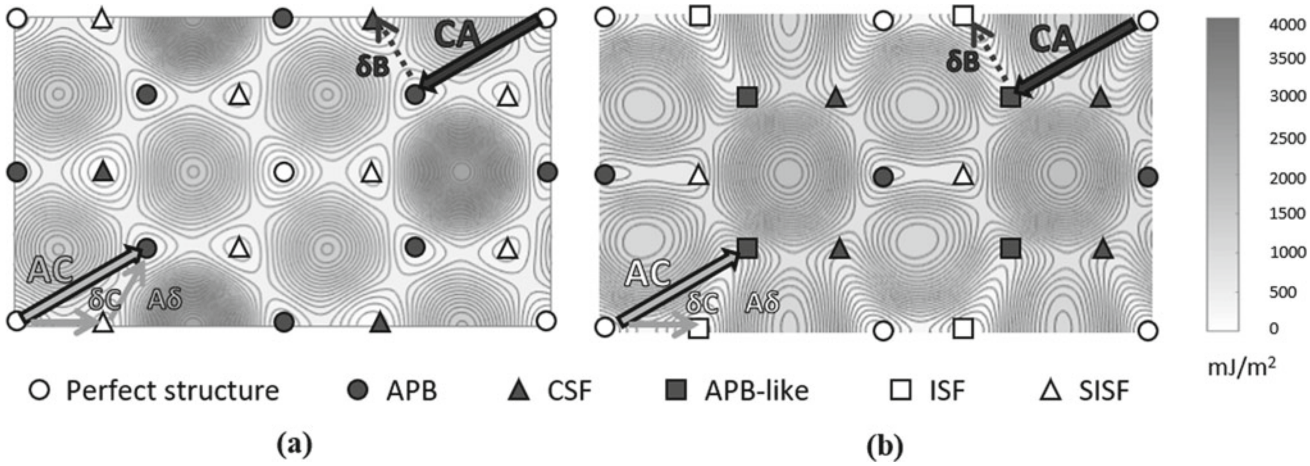

Fig. 4 Deformation pathways in **a** γ' and **b** γ'' phases created by individual a/2 <110> dislocations shown in Fig. 3

and the remnant partial δB stay in the γ phase. The final deformation microstructure is perfect crystal structure in both phases with δA + δB partial dislocations looping the γ'' particles. The deformation pathways are plotted by the dark gray arrows in Fig. 7. It should be noted that an extra APB is formed in the γ' phase due to the existence of the remnant Shockley partial δB, which is in contrast with the regular APB ribbon created by coupled a/2 <110> dislocations in a monolithic γ' particle (dash light gray arrows on Fig. 7a). This could provide additional strengthening effect.

Shearing of a Dual-Lobed Co-precipitate by an a/2 <112> Dislocation Group (i.e., AC + AB)

Figure 6 shows the interaction between an AC + AB (a/2 <112>) dislocation group and the dual-lobed co-precipitate. In the γ' phase, AC first creates an APB (Frame 1) and then an SISF is formed by the leading partial of AB (Frame 2). The trailing partial of AB finally cuts into the γ' phase and leaves an APB. In the γ'' phase, a remnant Shockley partial is created, which loops around the γ'' particle, leaving an ISF in the particle. Unlike the remnant Shockley partial created by the a/2 <110> dislocation, this Shockley partial does not propagate into the γ' phase due to the high CSF energy. The deformation pathway is indicated by the solid light gray arrows in Fig. 7. The remnant Shockley partial δB is represented by the dash dark gray arrow.

Shearing of a Dual-Lobed Co-precipitate by an a <112> Dislocation Group (i.e., AC + AB + AC + AB)

In order to study the effect of the remnant Shockley partial created by the a/2 <112> dislocation group, another set of simulations is performed for a <112> dislocation group (i.e., 2 sets of AC + AB) with and without the formation the remnant Shockley partial. Figure 8a shows the interaction between the two sets of coupled a/2 <112> dislocation group with the dual-lobed co-precipitate. In the γ' phase, the deformation pathway is shown by the solid light gray arrows

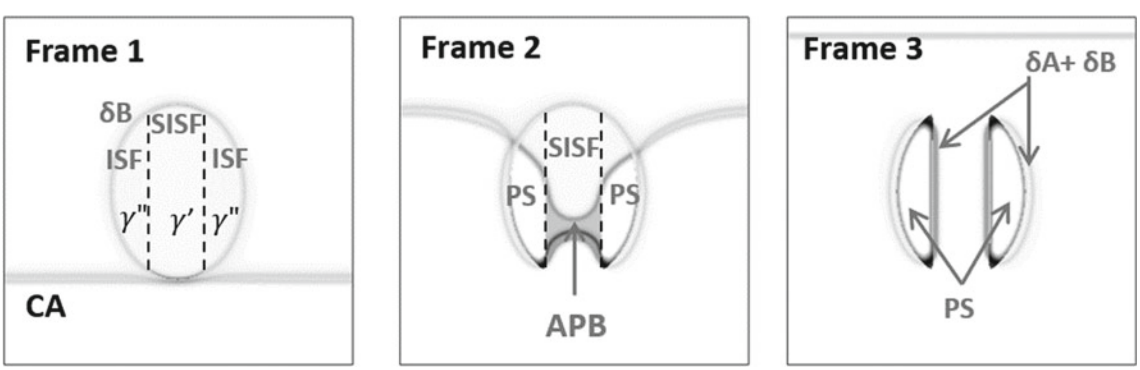

Fig. 5 Interaction between a second CA dislocation with the dual-lobed co-precipitate that has been sheared by a CA dislocation. PS represents perfect crystal (i.e., without the presence of any faults)

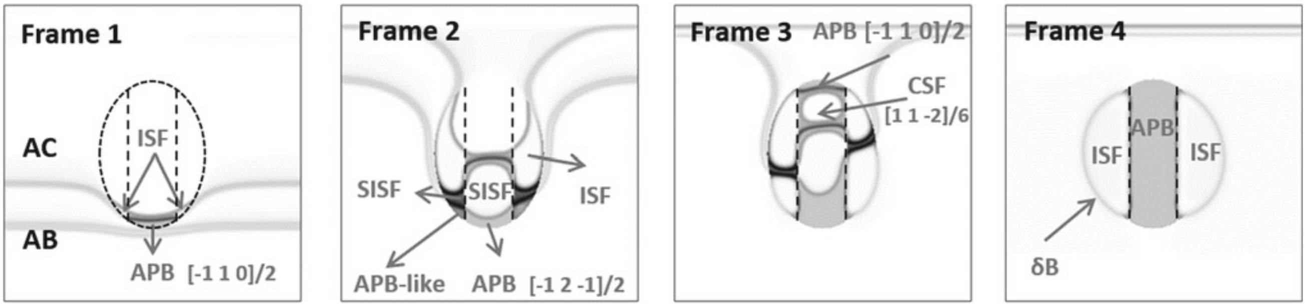

Fig. 6 Interaction between an AC + AB (a/2 <112>) dislocation group with the dual-lobed co-precipitate

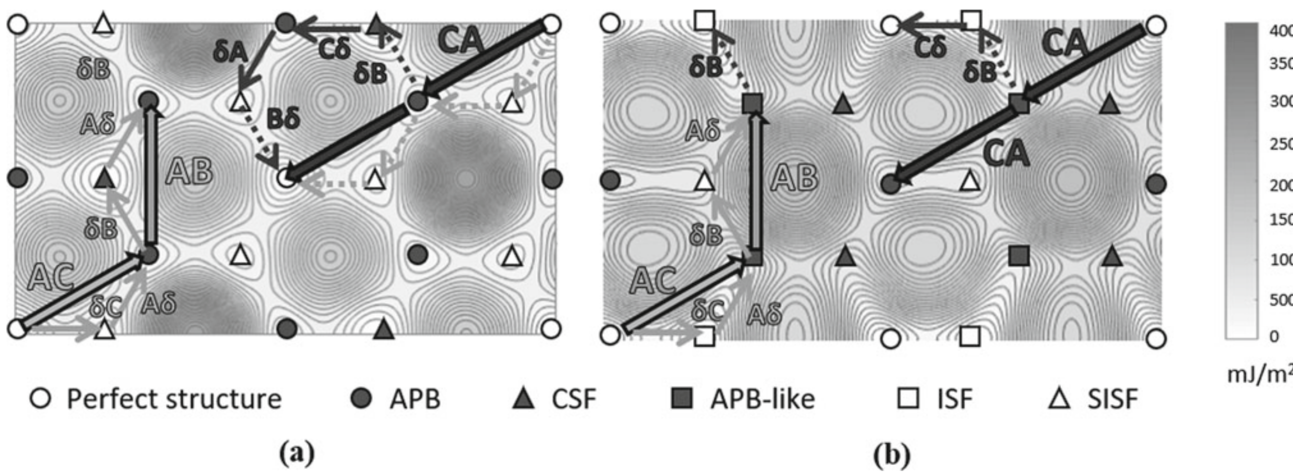

Fig. 7 Deformation pathways in **a** γ' and **b** γ'' phases created by a pair of like-signed and dislike-signed a/2 <110> dislocations shown in Figs. 5 and 6

in Fig. 9a. Various faults along the pathway (APB-SISF-APB-CSF-APB) are identified in the inset of the intermediate frame in Fig. 8a. In the γ'' phase, since the first AB and second AC are strongly coupled, no nucleation of remnant Shockley partial is observed. The deformation pathway is shown by the solid light gray arrows in Fig. 9b. Figure 8b shows the interaction between the second set of a/2 <112> dislocation group and the dual-lobed co-precipitate, assuming the first set has already passed, and the remnant Shockley partial has nucleated. The deformation of the γ' phase is not affected by the remnant partial since it does not enter the γ' phase. But in the γ'' phase, instead of forming the high-energy CSF, a perfect crystal structure (without any fault) is restored after the second AC cuts in (insets of the intermediate frame). The deformation pathway is shown by the dark gray arrows in Fig. 9b. The unstable CSF is eliminated by nucleating another remnant Shockley partial Bδ, which annihilates with the previous remnant Shockley partial δB. The final deformation microstructure is perfect crystals (i.e., without any faults) in both phases and an AB dislocation looping around the γ'' particles. It is worth noting that the remnant Shockley partial changes the deformation pathway but does not change the final deformation microstructure.

Another effect of the remnant Shockley partial created after the a/2 <112> dislocation group is on the dissociation sequence of the a/2 <110> dislocations in the γ matrix. Figure 10 shows a comparison of dislocation dissociation behavior with and without the remnant Shockley partial δB. Without the remnant Shockley partial, each a/2 <110> dislocation dissociates as the white arrows indicate in Fig. 10c. With the remnant Shockley partial δB, however, the dissociation sequence of the second set of AC + AB is shown by the solid dark gray arrows in Fig. 10c. Because the leading partial of the second AB is the same as the remnant Shockley partial, they will merge. Consequently, the trailing partial Aδ of the second AC must be the leading partial, which is clearly indicated by the dislocation node in Fig. 10b. The dissociation sequence of the second set of AC + AB dislocation is indicated by the dark gray arrows in Fig. 10c.

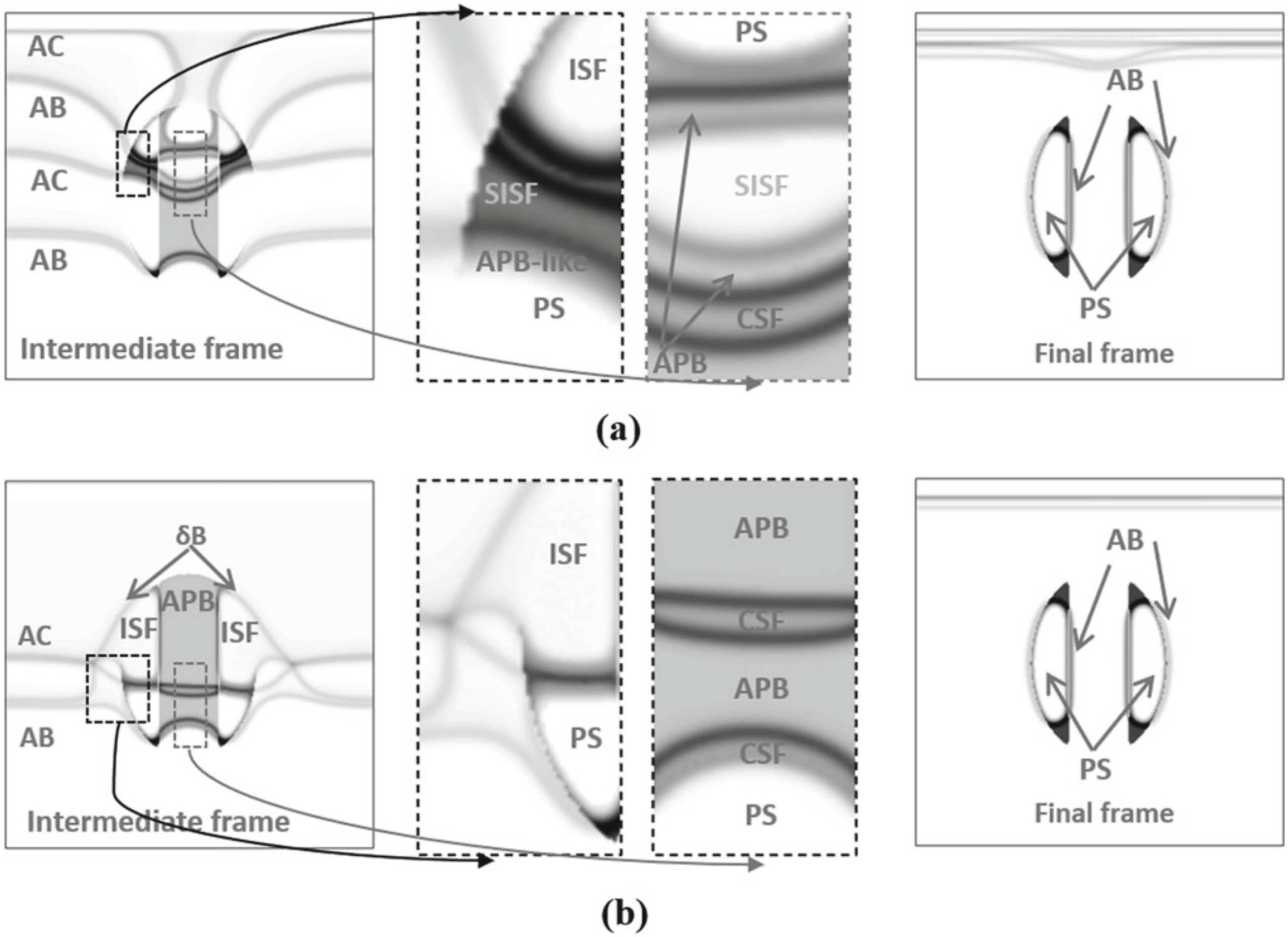

Fig. 8 Interaction between two sets of AC + AB (*a* <112>) dislocation group with the dual-lobed co-precipitate, if the two sets are **a** closely coupled and **b** decorrelated

Discussion

Experimental Characterization of Fault Structures

Some fault configurations that have been found in the simulations are difficult to identify experimentally by atomic resolution imaging, e.g., when only APB faults or perfect structure are left behind in the co-precipitates or when the Burgers vector of the dislocation that sheared the co-precipitate is parallel to the viewing direction. The offset of the γ'/γ'' interface is sometimes larger than what would be produced by shear of a single *a*/2 <110> dislocation. The fault configurations in such cases indicate that they might have been produced by *a*/2 <110> dislocations of unlike burgers vectors. Low magnification images can be utilized to further prove the co-existence of multiple dislocation types. Figure 11 shows a series of dislocations piling up on a single shear plane. The Burgers vector of each dislocation was determined. It was shown that three dissociated dislocations were present. Two of these dislocations had a net Burgers vector consistent with a screw 1/2 <110> dislocation. The third has mixed character with a net projected Burgers vector pointed to the right in the figure. This evidence directly shows that a single slip system will have multiple types of dislocations active under a single imposed shear stress. Evidence for multiple 1/2 <110> dislocations was found in samples deformed across the entire temperature range. This certainly provides confidence that the fault configuration ISF/APB/ISF reported in the literature [19] could very likely be a result of a pair of unlike-signed *a*/2 <110> dislocation group shearing the co-precipitate.

So far, all configurations that have been analyzed in the experiment can be well explained by the phase field simulation results presented herein. A more detailed comparison of model prediction and experimental finding is ongoing, and the results will be published in a follow-up study.

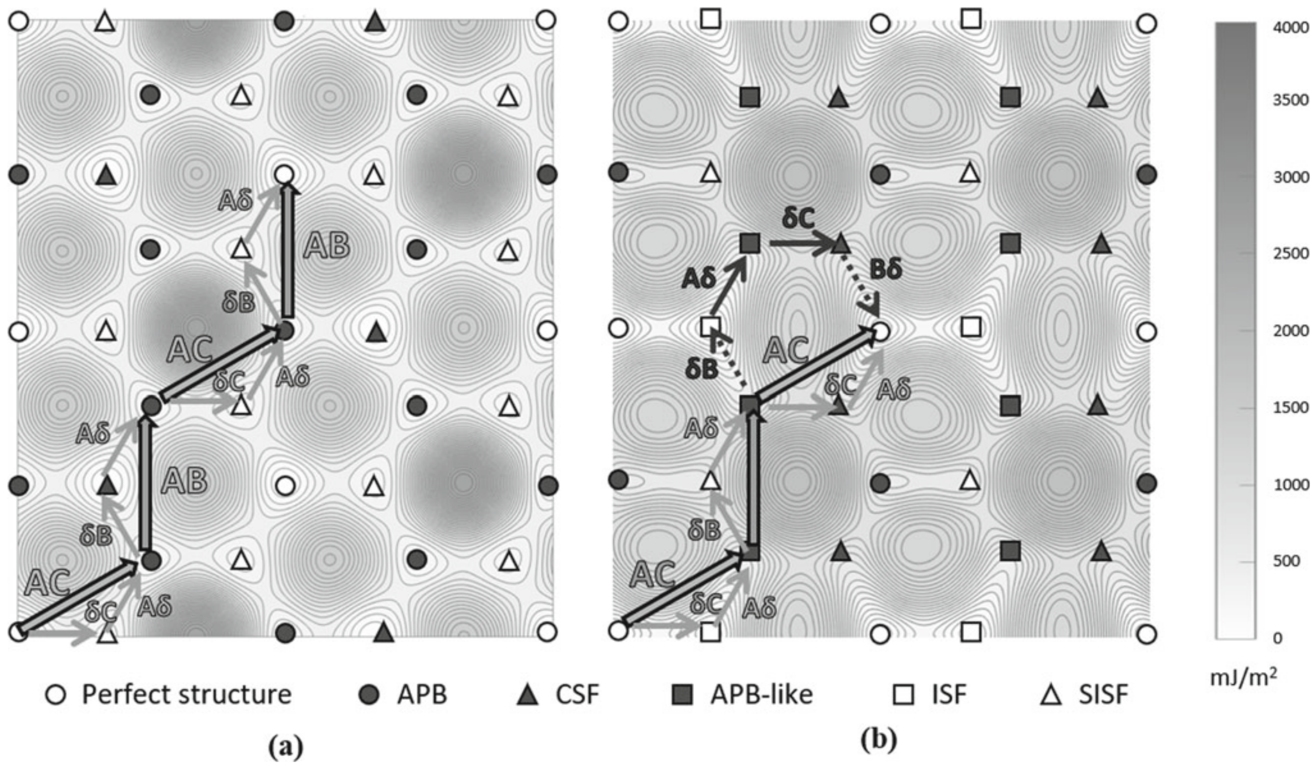

Fig. 9 Deformation pathways in **a** γ' and **b** γ'' phases created by two sets of AC + AB (*a* <112>) dislocation group shown in Fig. 8

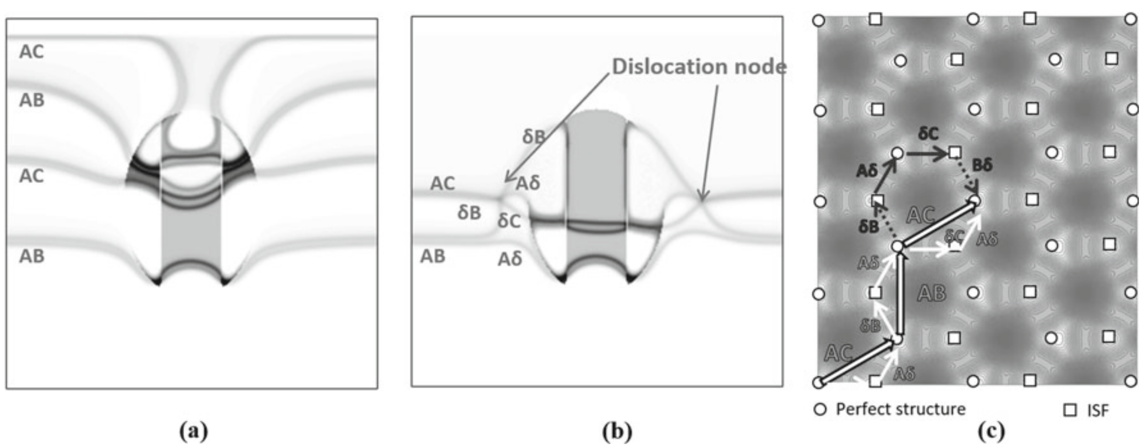

Fig. 10 Intermediate frame of **a** closely coupled and **b** decorrelated *a* <112> dislocation group interacting with the dual-lobed co-precipitate. **c** The dissociation sequences of the *a* <112> dislocation group shown in Fig. 10a, b

On the Interplay Between γ' and γ'' Deformation in the Shearing of a Co-precipitate

One of the motivations to study the deformation behavior of a co-precipitate is to find out if the deformation mechanisms of a co-precipitate are different from those found in monolithic precipitates of both phases, i.e., if there are some coupling effects between the deformation processes of the γ' and γ'' phases in a composite particle. The interaction between the CA dislocations and the dual-lobed co-precipitate has shown clearly this coupling effect. After the first CA dislocation passes the microstructure, a remnant Shockley partial δB nucleated in the γ'' phase cuts into the γ' phase and transforms the APB in it into an SISF (Fig. 3c). This extended fault itself is interesting because the Burgers vector of the dislocation from the matrix is *a*/2 <110> type, but the deformation pathway within the co-precipitate is effectively along <112>. This could never occur in

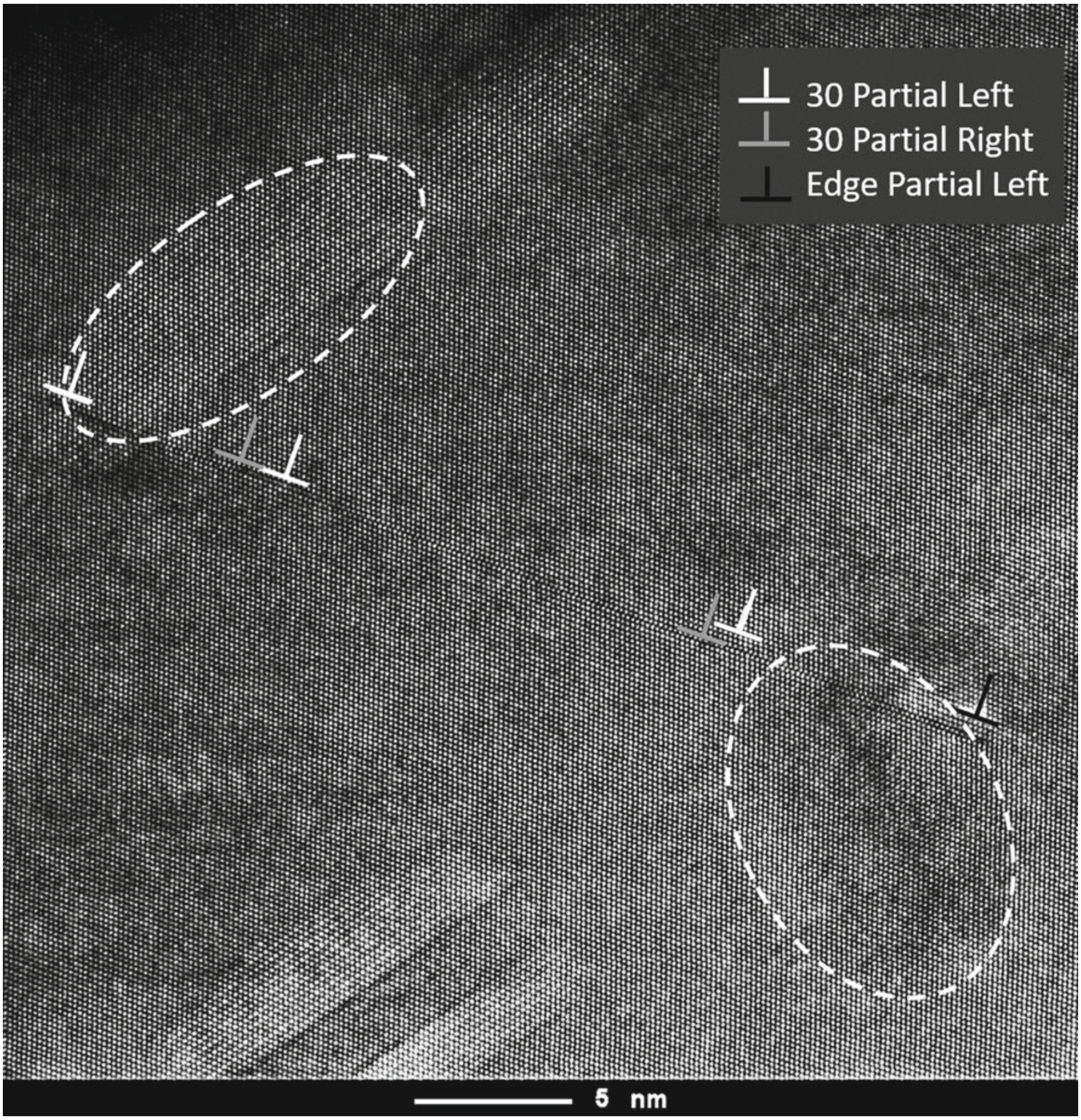

Fig. 11 STEM-HAADF micrograph along *a* <110> zone axis of a tensile specimen (T = 429 °C, $\dot{\varepsilon} = 3 \times 10^{-5} s^{-1}$, $\varepsilon = 0.5\% \sim 1\%$). Dislocations of different character are active on the same glide plane and are situated close to the γ''/γ and γ'/γ interfaces of the sheared co-precipitates (the white dash ellipse sketches the rough matrix/co-precipitate boundary). Three dissociated ½ <110> dislocations of which two are likely screw type and one is of mixed type were identified. Their location is shown with a few stacking faults extending through all three phases

γ'-strengthened alloys. If the γ' and γ'' precipitates are well-separated (i.e., in the cases of monolithic precipitates), we would not expect to see this mechanism operating either. This is because the remnant Shockley partial δB will not expand into the γ matrix when the applied stress is perpendicular to its Burgers vector. If δB does not expand into the matrix, it will not encounter the γ' particles. Lv et al. [10] have showed that the remnant Shockley partials loop γ'' particles and stay at the γ/γ'' interfaces for individual γ'' precipitates. Moreover, the expansion of the remnant Shockley partial loop into the γ' phase leads to the change of the deformation pathway of the second CA dislocation and the formation of an additional APB in the γ' phase (see the deformation pathway drawn on Fig. 7a). The additional strengthening effect from this additional APB is therefore unique in the co-precipitate case.

The coupling effect can be shown more quantitatively with a normalized strain–time plot. Figure 12a shows the strain–time plot for four precipitate microstructures interacting with an AB dislocation. Besides the dual-lobed precipitate microstructure, a single monolithic γ' or γ'' precipitate with the same shape as the co-precipitate are

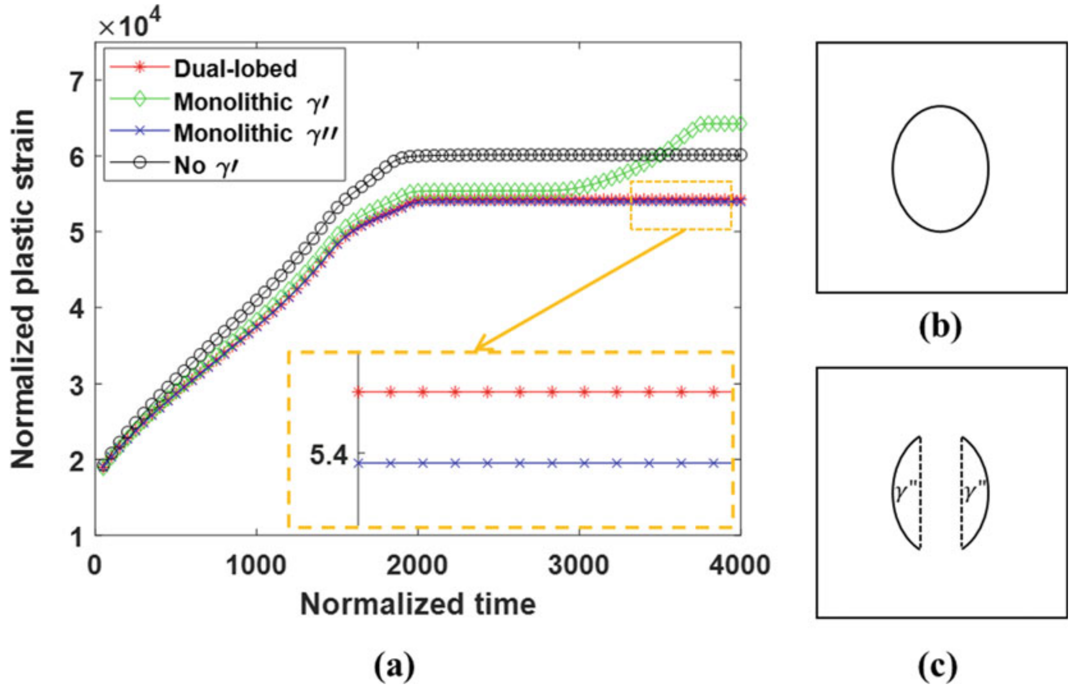

Fig. 12 **a** Normalized strain–time plot for four different precipitate microstructures. **b** Precipitate microstructure used for single monolithic γ' and γ'' phases. **c** Precipitate microstructure used without γ' in the middle, dubbed "no-γ'" in Fig. 12a

considered (see Fig. 12b). The microstructure in Fig. 12c shows a precipitate configuration created by removing the γ' particle from the co-precipitate, leaving a γ-channel in between two γ'' particles (dubbed "no γ'" in Fig. 12a). From the strain–time plot, it is seen that without the γ' in the middle, the strain rate is the fastest (black circles) because the precipitate volume fraction of the no-γ' configuration is smaller than that in the rest three cases and the γ'' particles have sharp edges. With the same precipitate volume fraction, the monolithic γ' (green diamonds) microstructure has the largest plastic strain while the monolithic γ'' (blue crosses) microstructure has the smallest plastic strain. This is because the APB energy in the γ' phase is much smaller than that in the γ'' phase. Thus, during the deformation, the AB dislocation shears the monolithic γ' particle, but loops the monolithic γ'' particle. What is more interesting is that the plastic strain for the dual-lobed structure (red asterisks) is almost the same as that for the monolithic γ'' microstructure. Even though there is a γ' layer in the middle in the co-precipitate, the AB dislocation still cannot shear through the particle because of the γ'' on the outside. The dislocation enters the γ' phase just a little bit from the γ/γ' interface, which is why the curve with the red asterisks is slightly higher than that with the blue crosses in the inset of Fig. 12a. This will not happen if γ' and γ'' are well separated. This suggests that the dual-lobed microstructure can in some way behave like a large γ'' particle as if the middle is not γ'. However, one may not be able to obtain monolithic γ'' particles with the size and aspect ratio resemble those of the dual-lobed particles. This certainly offers some new perspectives on how co-precipitates may improve the strength of the alloy.

Another important coupling effect is the misfit among any two of the three co-existing phases, i.e., γ, γ' and γ''. Previous simulation results [19] have shown the stress field of a co-precipitate and concluded that the elastic interaction between γ' and γ'' is such that they prefer to form co-precipitate (i.e., self-accommodating the misfit strain). Even though the total elastic energy is reduced by having a co-precipitate rather than separate particles, the stress field of a composite particle is more complicated than that of a monolithic particle of either phase. Due to misfit, the γ/γ'' interface has high positive stress levels whereas the γ/γ'' interface has medium negative stress levels for dilatational stress. The dual-lobed precipitate would then possess a stress field with alternating positive and negative values at the precipitate–matrix interface [19], which possibly could have significant and interesting effects on dislocation motion at the precipitate–matrix interface. This will be addressed in the follow-up work.

Conclusions

We have investigated the deformation pathways of a dual-lobed co-precipitate in IN718 Ni-base superalloys by using a microscopic phase field model with ab initio calculations of the generalized stacking fault energy as inputs. The interplay between the shearing processes of γ' and γ'' particles in the co-precipitate further complicates the already complicated deformation processes of the individual precipitates. An ISF/APB/ISF fault configuration observed in the experiment can be created either by a single AC (*a*/2 <110>) dislocation or by an AC + AB (*a*/2 <112>) dislocation group. An extended fault within the dual-lobed co-precipitate is created by a single CA dislocation where a remnant Shockley partial δB created in the low symmetry γ'' phase enters the γ' phase and stays at particle–matrix interface. An additional APB is formed by the interaction between an CA + CA dislocation group and the co-precipitate. The remnant Shockley partial also changes the dissociation sequence of the matrix dislocations. The experiment difficulty in characterizing fault structures in the co-precipitates and the coupling effect between the γ' and γ'' phases are discussed. The mechanisms uncovered above may shed some light on the strengthening effect of the co-precipitates in Alloy 718.

Acknowledgements The authors would like to acknowledge the financial support from NSF DMREF program under grant DMR-1534826. CHZ acknowledges sponsorship provided by the Alexander von Humboldt foundation through a Feodor-Lynen Research Fellowship.

References

1. Carlson R. G, Radavich J. F (1989) Microstructural characterization of cast 718. In International Symposium on Superalloys (pp. 79–95).
2. Rao G. A, Kumar M, Srinivas M, Sarma D. S (2003) Effect of standard heat treatment on the microstructure and mechanical properties of hot isostatically pressed superalloy inconel 718. Materials Science and Engineering: A: 355(1–2), 114–125.
3. Baccino R, Moret F, Pellerin F, Guichard D, Raisson G (2000) High performance and high complexity net shape parts for gas turbines: the ISOPREC® powder metallurgy process. Materials & Design: 21(4), 345–350.
4. Kovarik L, Unocic R. R, Li J, Sarosi P, Shen C, Wang Y, Mills M. J (2009) Microtwinning and other shearing mechanisms at intermediate temperatures in Ni-based superalloys. Progress in Materials Science: 54(6), 839–873.
5. Pollock T. M, Field R. D. (2002) Dislocations and high-temperature plastic deformation of superalloy single crystals. In Dislocations in solids (Vol. 11, pp. 547–618). Elsevier.
6. McAllister D, Lv D, Peterson B, Deutchman H, Wang Y, Mills M. J (2016) Lower temperature deformation mechanisms in a γ''-strengthened Ni-base superalloy. Scripta Materialia: 115, 108–112.
7. Vorontsov V. A, Shen C, Wang Y, Dye D, Rae C. M. F (2010) Shearing of γ' precipitates by <1 1 2> dislocation ribbons in Ni-base superalloys: A phase field approach. Acta Materialia: 58 (12), 4110–4119.
8. Zhou N, Shen C, Mills M. J, Li J, Wang Y (2011) Modeling displacive–diffusional coupled dislocation shearing of γ' precipitates in Ni-base superalloys. Acta Materialia: 59(9), 3484–3497.
9. Feng L, Lv D, Rhein R. K, Goiri J. G, Titus M. S, Van der Ven A, Pollock T. M, Wang, Y. (2018). Shearing of γ'particles in Co-base and Co-Ni-base superalloys. Acta Materialia: 161, 99–109.
10. Lv D. C, McAllister D, Mills M. J, Wang Y (2016) Deformation mechanisms of D022 ordered intermetallic phase in superalloys. Acta Materialia: 118, 350–361.
11. Oblak J. M, Paulonis D. F, Duvall D. S (1974) Coherency strengthening in Ni base alloys hardened by DO 22 γ' precipitates. Metallurgical Transactions: 5(1), 143.
12. Sundararaman M, Mukhopadhyay P, Banerjee S (1988) Deformation behaviour of γ''strengthened Inconel 718. Acta Metallurgica: 36(4), 847–864.
13. Miller M. K, Babu S. S, Burke M. G (2002) Comparison of the phase compositions in Alloy 718 measured by atom probe tomography and predicted by thermodynamic calculations. Materials Science and Engineering: A: 327(1), 84–88.
14. Cozar R, Pineau A (1973) Morphology of γ'and γ" precipitates and thermal stability of inconel 718 type alloys. Metallurgical Transactions: 4(1), 47–59.
15. Theska F, Stanojevic A, Oberwinkler B, Ringer S. P, Primig S (2018) On conventional versus direct ageing of Alloy 718. Acta Materialia: 156, 116–124.
16. Theska F, Nomoto K, Godor F, Oberwinkler B, Stanojevic A, Ringer S. P, Primig S (2020) On the early stages of precipitation during direct ageing of Alloy 718: Acta Materialia, 188, 492–503.
17. Andrieu E, Wang N, Molins R, Pineau A (1994) Influence of compositional modifications on thermal stability of alloy 718. Superalloys: 718, 625–706.
18. Shen C, Wang Y (2003) Phase field model of dislocation networks. Acta materialia: 51(9), 2595–2610.
19. McAllister D, Lv D, Feng L, Deutchman H, Wessman A, Wang Y, Mills M. J (2018) Characterization and modeling of deformation mechanisms in Ni-base superalloy 718. In Proceedings of the 9th International Symposium on Superalloy 718 & Derivatives: Energy, Aerospace, and Industrial Applications (pp. 319–338). Springer, Cham.